

Experimental models of salivary gland cancer established using organoid culture and patient-derived xenografting

Yoshihiro Aizawa

Yokohama City University

Kentaro Takada

Yokohama City University

Jun Aoyama

Yokohama City University

Daisuke Sano (✉ dsano@yokohama-cu.ac.jp)

Yokohama City University

Shoji Yamanaka

Yokohama City University Hospital

Masahide Seki

The University of Tokyo

Yuta Kuze

The University of Tokyo

Jordan Ramilowski

Yokohama City University

Ryo Okuda

Roche Pharma Research and Early Development, Roche Innovation Center Basel

Yasuharu Ueno

the University of Tokyo

Yusuke Nojima

Yokohama City University

Yoshiaki Inayama

Yokohama City University Medical Center

Hiromitsu Hatakeyama

Yokohama City University Graduate School of Medicine

Takashi Hatano

Yokohama City University

Hideaki Takahashi

Yokohama City University

Goshi Nishimura

Yokohama City University

Satoshi Fujii

Yokohama City University Graduate School of Medicine

Yutaka Suzuki

The University of Tokyo

Hideki Taniguchi

the University of Tokyo

Nobuhiko Oridate


Yokohama City University

Research Article

Keywords: salivary gland cancer, organoid culture, patient derived xenograft (PDX) model, patient-derived organoid, PDX-derived organoid

Posted Date: May 11th, 2022

DOI: <https://doi.org/10.21203/rs.3.rs-1621957/v1>

License:  This work is licensed under a Creative Commons Attribution 4.0 International License. [Read Full License](#)

Abstract

Purpose: Salivary gland carcinoma (SGC) has poor prognosis depending on the histological subtype. However, due to the scarcity of preclinical experimental models, its molecular biology remains largely unknown, hampering the development of new treatment modalities for patients with these malignancies. The aim of this study is to generate human SGC experimental models for multiple histological subtypes using patient-derived xenograft (PDX) and organoid culture techniques.

Methods: Tumor specimens from surgically resected SGC were proceeded for the preparation of PDX and patient-derived organoid (PDO). Specimens from SGC PDX were also proceeded for PDX-derived organoid (PDXO). *in vivo* tumorigenicity was assessed by orthotopic transplantation of SGC organoids. The pathological characteristics of each model were compared to those of the original tumor by Immunohistochemistry analysis. The genetic traits of PDO samples were analyzed by RNA-seq.

Results: A series of SGC PDOs, PDX and PDXO models using human SGC tumor section for salivary duct carcinoma, mucoepidermoid carcinoma, and myoepithelial carcinoma were successfully generated. Through passaging, each model was confirmed to almost maintain the pathological characteristics of the original tumor and the genetic traits including transcription profiles, genomic variation and the presence of fusion genes of corresponding histological subtypes.

Conclusion: We here described success in the generation of *in vitro* and *in vivo* SGC models of multiple histological subtypes using organoid culture and PDX, recapitulating the histological and genetical characteristics of original tumor. Thus, our experimental models of SGC could be a powerful resource for the development of novel therapeutic agents and investigating the molecular biology of these malignancies.

Introduction

Salivary gland carcinomas (SGCs) are uncommon malignancies, representing approximately 0.3% of all cancers, with the estimated annual incidence of 0.05 to 2 per 100,000 population[1]. These malignancies exhibit considerable pathologic, biological, and clinical diversity. Currently, there are 22 histological subtypes [2]; therefore, accurate preoperative diagnosis of these diseases has become quite difficult in clinical practice[3, 4]. Among the many histological subtypes, salivary duct carcinoma (SDC) is highly malignant with a high rate of distant metastatic recurrence and a 5-year survival rate of only 40%[5, 6]. Adenoid cystic carcinoma (ACC) is one of the most common histological subtypes of SGCs, characterized by high rate of perineural invasion, local recurrence, and delayed onset of distant metastases[7, 8]. The prognosis of mucoepidermoid carcinoma (MEC), another common type of SGCs, is highly dependent on the pathological grade, with a 5-year survival rate of 22.5% in high-grade cases, and a majority of patients die from distant metastasis rather than local recurrence[9, 10]. Thus, patients diagnosed with some aggressive histological subtypes of SGCs represent poor prognosis.

Despite this background, the disease pathogenesis of SGCs remains unclear[11], except in cases of tumor-specific recurrent chromosomal translocations that result in the formation of fusion genes, such as *CRTC1 [MECT1]-MAML2* identified in MEC[12] or *MYB-NFIB* in ACC[13]. The lack of *in vitro* and *in vivo* SGC models that can effectively recapitulate the diversity of human SGC has hampered the understanding of disease progression.

Recently, patient-derived xenograft (PDX) and organoid cultures have emerged as useful preclinical tools to overcome problems in traditional two-dimensional culture by mimicking traits and heterogeneity of the original tumor[1, 14]; these technologies have the potential to be a stepping stones to personalized medicine[15, 16]. We previously reported the successful establishment of ACC patient-derived organoids (PDOs), short-term organoids from ACC PDX (PDXOs of ACC), and organoids-transplanted animal model of ACC, reproducing the histological characteristics of original tumor, and showed the significance of our model for drug screening evaluation[17]. Here, we established multiple experimental models of SGCs, including SDC, MEC, and myoepithelial carcinoma (MYEC), using organoid culture and patient-derived xenografting. Additionally, we genetically characterized these novel models of SGC using RNA-seq analysis.

Materials And Methods

Human Specimens

We obtained 40 fresh SGC tumor tissues from patients undergoing surgical resection at Yokohama City University Hospital or Yokohama City University Medical Center (Yokohama, Japan) and stored them in culture medium on ice until further use (< 12 h). The pathological diagnosis for each case was confirmed by independent pathologists after sample collection. We obtained written informed consent from all patients prior to surgery.

Patient-derived xenografts (PDX)

PDX were established by subcutaneous implantation of fresh minced tumors into NOD Cg-Prkdc^{scid} Il2rg^{tm1Wjl}/SzJ (NSG) mice as previously described²⁰. All mice were dissected to visually examine for metastases in lung, liver, and abdominal cavity.

Organoid culture

Organoid cultures from patient specimens and PDX were performed as previously described[17–19]. Briefly, the tissue, cut into 2–4 mm pieces, was enzymatically digested with Liberase TM Research Grade (Sigma Aldrich, St. Louis, MO, USA) and Hyaluronidase (Sigma Aldrich) for 30–60 min at 37°C. Processed tissue was passed through a 70 µm cell strainer (Corning Incorporated, Corning, NY, USA) to eliminate macroscopic pieces. The isolated cells were suspended in complete media and seeded on growth-factor-reduced (GFR) Matrigel (Corning Incorporated) coated plate, pre-prepared as a lower layer as previously described[17]. In this procedure, 6, 12, 24 and 48 wells plates were used according to cell quantity. After incubation for 16–24 hours, the media was removed and the organoids formed on the lower layer were covered with additional GFR Matrigel as an upper layer. The complete media was added after the formation of solid coating, and the media was changed every 2–3 days. For passaging, the Matrigel containing organoids was collected from the plate, and digested with TrypLE Express Enzyme (Thermo Fisher Scientific, Waltham, MA, USA) for about 5 to 10 minutes. Isolated organoids were suspended in DMEM/F12 media and physically crushed into smaller cell clumps by pipetting. Cells were centrifuged, re-suspended in complete media with 10 µM ROCK inhibitor (Y-27632, Sigma), and then embedded in GRF Matrigel as described above. Organoids were passaged at a 1:2 to 1:1.5 dilution ratio every 2–3 weeks. To prepare frozen stocks, organoids were isolated and suspended in CELLBANKER 1 (TAKARA-BIO, Kusatsu, Shiga, Japan) and stored in – 80°C freezer or liquid nitrogen. Stocks have been successfully recovered for up to at least 6 months after freezing. STR analysis was performed at BEX. CO., LTD. (Tokyo, Japan) to authenticate the identity

of organoids and corresponding patient tissue. To check the contamination of mouse cells, we performed PCR of animal species-specific mitochondrial DNA sequences[20] using the primers listed in Supplementary Table S3.

Transplantation of organoids

For orthotopic transplantation of SGC organoids, organoids were injected into the submandibular gland in NSG mice as previously described[17]. The submandibular gland was injected with 0.5×10^5 to 1×10^6 cells suspended in a mixture of DMEM/F12 media and Matrigel. For subcutaneous transplantation of SGC organoids, organoid suspension (1 to 2×10^6 cells) were similarly injected into the flank subcutaneously in NSG mice. Tumor volumes were measured weekly. Xenografts were harvested when the tumor diameter reached > 1 cm or 6 months after implantation and fixed for 24 h in 10% formalin.

Immunohistochemistry analysis

Fresh PDXs and orthotopically transplanted organoids were fixed in 10% formalin for 24 h and then embedded in paraffin following standard histological procedures. Organoids were isolated by digesting Matrigel using dispase (Sigma) for 30 min at 37°C and embedded into a gel using iPGell (GenoStaff, Tokyo, Japan) according to the manufacturer's protocol. Next, the organoids were fixed in 10% formalin for 24 h and paraffin-embedded. Haematoxylin–eosin staining and Immunohistochemistry (IHC) were performed using standard protocols on 5- μ m-thick paraffin sections. The following antibodies were used for IHC: human-Androgen Receptor (AR441, Dako, Carpinteria, CA, USA) 1:500, pan keratin AE1/AE3/PCK26 (Roche, Basel, Switzerland) 1:1, HER2 (4B5, Roche) 1:1, alpha-smooth muscle actin (S131, Leica Biosystems, Buffalo Grove, IL, USA) 1:1, p63 (4A4, Biocare medical, Concord, CA, USA) 1:200, S-100 (Roche) 1:1000, and GCDFP15 (D6, Biocare medical) 1:400. Images were acquired using an OLYMPUS BX41 microscope.

DNA/RNA extraction

Organoids were extracted from Matrigel using TrypLe. Total RNA was extracted from organoids using TRIzol (Thermo Fisher), followed by isolation and precipitation in chloroform and 70% ethanol, and then purified via column-based separation using the RNeasy Mini Kit (QIAGEN, Valencia, CA). DNA was extracted from organoids using DNA mini kit (QIAGEN) according to the manufacturer's protocol. PDX tissues harvested from mice, as well as tissue fragments of primary salivary gland tumor, were physically homogenized using a plastic homogenizer pestle. RNA and DNA extraction from these homogenized tissues were processed similarly as described above. STR analysis was performed as described above.

RNA-seq

RNA sequencing was performed at the Laboratory of Systems Genomics, Department of Computational Biology and Medical Sciences, at the University of Tokyo (Chiba, Japan). RNA quality and quantity were measured with an Agilent Bioanalyzer 2100. Libraries for sequencing were constructed using TruSeq Stranded mRNA (Illumina, San Diego, CA, USA) according to the manufacturer's protocol, followed by sequencing on an Illumina NovaSeq6000 platform to generate 70 million paired-end reads of 150 bases. The RNA-seq data are available at the DNA Data Bank of Japan Sequence Read Archive (DRA) under the accession number DRA011243.

Gene expression analysis

RNA-seq reads were quality checked and adapter trimmed using fastp (v0.20.1)[21]. Since RNA-seq reads derived from PDX tumors and PDXOs both essentially contain mouse reads, we distinguished the trimmed reads into

those of humans (GRCh38/hg38) or mice (GRCm38/mm10) using xenome (v1.0.0)[22]. Only human reads were used for subsequent processing. Mouse reads and indistinguishable reads were discarded. To ensure consistency in process sampling, samples that do not contain intrinsic mouse reads, such as patient-derived organoids, were processed in the same manner as described above. The human reads were aligned to human genome reference sequence (GRCh38/hg38) using STAR (v2.7.5c)[23] and counted for each gene using featureCounts (v2.0.1)[24]. The RNA-seq coverage and quality statistics are summarized in Supplementary Table S3. For a heatmap, hierarchical clustering analysis with complete linkage and Euclidean distance, and correlation analysis, the raw read counts per gene with at least an average of 5 counts were TMM normalized using edgeR (v3.30.3)[25] and log2-transformed. The heatmap and clustering analysis were visualized with the top 2000 variable genes using R package "pheatmap." The Pearson's correlation coefficients were calculated for all genes. For a principal component analysis (PCA), we combined our samples with RNA-seq datasets of multiple salivary gland cancers downloaded from public databases. SRP067524 (including 42 samples of ACC and 5 samples of normal salivary gland), SRP067827 (including 3 samples of acinic cell carcinoma), SRP096726 (including 16 samples of SDC), and SRP109264 (including 40 samples of MEC) were downloaded from the NCBI Sequence Read Archive. The raw read counts per gene for all samples were calculated as described above and were normalized for library size by converting to CPM (counts per million) using edgeR[25]. The R package "sva" (v3.36.0)[26] was applied to adjust for batch effects, along with information of histological subtype of each sample. PCA was performed using the "prcomp" function in R.

Variant calling

Single Nucleotide Polymorphism (SNP) discovery and filtering from RNA-seq data were performed using HaplotypeCaller under standard parameters according to GATK[27] (v4.1.8) Best Practices (<https://github.com/gatk-workflows/gatk3-4-rnaseq-germline-snps-indels>). Additionally, SNPs with a depth < 25 and an allele frequency < 0.2 were excluded. The functional effects of the mutations were predicted using SnpEff (v5.0)[28], and SNPs with "high" or "moderate" functional importance were retained. To visualize representative genes that are mutated in salivary gland tumors in COSMIC[29], the vcf format data was converted to maf format data using ANNOVAR[30] and annovarToMAF under standard parameters, and the "waterfall" function of R package GenVisR (v1.20.0)[31] was applied.

Detection of fusion genes

Candidate fusion genes were explored from RNA-seq data using STAR-Fusion (v1.6.0)[23], FusionCatcher (v1.20)[32], and a combination of kallisto (v0.46.2)[33] and pizzly (v0.37.3)[34]. The detected candidate fusion genes were cross-referenced to ChimerDB4.0[35], and those reported in salivary gland carcinoma were extracted and validated by RT-PCR. RT-PCR was performed as previously described[17] using PrimeScript 1st strand cDNA Synthesis Kit (TAKARA-BIO), and RT-PCR products were subjected to Sanger sequencing at MacroGen Japan (Tokyo, Japan). All primers used are listed in Supplementary Table S4.

Mycoplasma detection

Organoids were routinely tested for Mycoplasma using e-Myco VALiD Mycoplasma PCR Detection Kit (iNtRON Biotechnology, Seoul, Korea). All experiments were performed with mycoplasma-free cells.

Statistical analysis

The association between the establishment rate of each experimental model and the clinical information of the patients was tested using Fisher's exact ratio test and Student's *t*-test in the open-source R Statistical Computing software (<http://www.r-project.org/>). Statistical significance was set at $P < 0.05$.

Results

SGC PDOs and PDX models

We established a series of SGC PDOs and PDX models using human SGC tumor section with multiple histological subtypes (Table 1) by our existing protocol for human-ACC derived organoid and PDX models[17]. Comprehensive clinical information of the patients involved in the present study is shown in Supplementary Table S1. As the overview of our examinations (Fig. 1), we aimed to establish both SGC PDO and PDX if enough tumor specimens were secured. Additionally, we sought to generate PDXO with *ex vivo* organoid culture of cells isolated from the established PDX tumors. PDX establishment was considered successful when two or more passages were possible, and organoid establishment was considered successful when five or more passages were possible and continuous growth was observed. Overall, we found that PDXs were established from 6 (20.7%) of the 29 patients, and PDOs were established from 4 (11.4%) of the 35 patients (Supplementary Table S1, the data included PDXs and PDOs from ACCs reported previously). It has to be noted that there were no instances of successful PDO culture without coincident PDX establishment except YCU-SDC-32. Additionally, PDXOs were generated from 3 (50.0%) of the 6 established PDXs (Supplementary Table S1).

Table 1
Patient characteristics.

Name	Sex	Age	Pathological diagnosis	Primary site	TNM stage (7th edition)			Last passage		
					T	N	M	PDX	Patient-derived organoid	PDX-derived organoid
YCU-ACC-1	F	48	Adenoid cystic carcinoma	Nasal cavity	4a	0	0	10 ^a	2 ^b	4 ^b
YCU-ACC-4	M	67	Adenoid cystic carcinoma	Sublingual gland	4a	2c	1	10 ^a	9 ^b	9 ^b
YCU-SDC-14	M	51	Salivary duct carcinoma	Submandibular gland	3	3b	0	8 ^a	55 ^a	35 ^a
YCU-MYEC-16	M	73	Carcinoma ex pleomorphic adenoma (Myoepithelial carcinoma)	Parotid gland	2	0	0	7 ^a	1 ^b	5 ^b
YCU-SDC-20	M	71	Salivary duct carcinoma	Parotid gland	4a	1	0	9 ^a	52 ^a	40 ^a
YCU-MEC-24	F	55	Mucoepidermoid carcinoma	Oral floor	4a	2b	0	5 ^a	25 ^b	35 ^a
YCU-SDC-32	M	72	Carcinoma ex pleomorphic adenoma (Salivary duct carcinoma)	Parotid gland	2	0	0	0 ^b	36 ^a	Not available
a As of March 2021.										
b Not being actively passaged at the time of publication.										

To date, four PDOs have been successfully established from patients with SDC (YCU-SDC-14, YCU-SDC-20, and YCU-SDC-32) and MEC (YCU-MEC-24) in this study. PDXs have been also established using SDC (YCU-SDC-14 PDX, YCU-SDC-20 PDX), MEC (YCU-MEC-24 PDX), and MYEC (YCU-MYEC-16 PDX). Additionally, PDXOs (YCU-SDC-14X, YCU-SDC-20X, and YCU-MEC-24X) have been successfully generated using YCU-SDC-14 PDX, YCU-SDC-20 PDX, and YCU-MEC-24PDX, respectively. The formation of SGC PDOs and PDXOs showed similar characteristics when aggregated on Matrigel according to their origins (Fig. 2 and Supplementary Fig. S1). Each generated organoid was confirmed to be a genetic match of the original tumor by short tandem repeat (STR) profiling. Thus, YCU-SDC-14, YCU-SDC-20, and YCU-MEC-24 specimens were able to generate PDOs, PDX models, and PDXOs (Table 1).

Our SGC PDX models were capable of up to 10 passages. YCU-SDC-14 PDX model often developed liver metastases after the first passage (Supplementary Fig. S2A). SGC PDOs and PDXOs were cultured at a passaging ratio of 1:1.5 to 1:2 approximately every 14 days, with up to 55 passages. These organoids and PDXs showed a

wide spectrum of proliferative activity, e.g. YCU-SDC-32 were able to passage more than 35 times as human tumor-derived organoid; however, the growth of PDX was slow, not yielding sufficient quantities for passaging of PDX or PDXO culture.

We did not observe any correlation between the establishment success rate for each model and clinical characteristics (data not shown). Our models were successfully recovered after the long-term preservation for at least 6 months in -80°C .

PDXs and orthotopic mouse model from SGC organoids retain their original histological features through passages

Next, we evaluated whether our SGC organoids and PDXs could recapitulate the histological characteristics of the original tumor. Most SGCs are usually well-differentiated tumors, resulting in difficult diagnosis with only a specific histological marker. Thus, it is necessary for us to look at a wide range of histological images to ensure an accurate diagnosis[10]. Since our *in vitro* organoids did not show sufficient histological structure, we first established an orthotopic animal model from our PDOs and PDXOs, as described previously[17], followed by histological analysis of orthotopically transplanted organoids. We confirmed palpable tumor formation 2–4 weeks after the transplantation (Fig. 1B), which required approximately six months to reach 1-cm tumor diameter.

Histologically, PDXs and orthotopic transplants from PDOs or PDXOs showed similar morphology to the originating SGC tumor, as confirmed by independent pathologists (Fig. 3 and Supplementary Fig. S2A–G). Highly differentiated structural characteristics of histological subtypes, such as cribriform structure with comedonecrosis in SDC (YCU-SDC-14 and YCU-SDC-20) and cystic structures lined by mucous cells and clear cells in MEC (YCU-MEC-24), were present in both PDXs and orthotopic transplants, as observed in the matched patient sample. Additionally, we observed that results of IHC for CK as an epithelial marker and p63 as a myoepithelial marker showed features similar to those in matched patient sample. Furthermore, PDXs and orthotopic transplants from PDOs or PDXOs retained the expressed human epidermal growth factor receptor 2 (HER2), which is frequently seen and is a possible potential therapeutic target in SDC. The expression of androgen receptor (AR) in the original tumor of YCU-SDC-14 was not retained with passaging in PDXs and orthotopically transplanted organoids. AR and GCDPF15 expression in the original tumor of YCU-SDC-20 was not confirmed for PDXs and orthotopically transplanted PDO; however, their expressions were retained in orthotopically transplanted PDXO. Overall, we confirmed that our all established organoids had the potential to generate orthotopic transplants and that these organoids and PDXs recapitulated the histological characteristics of the original tumor.

Transcription profiles of PDXs, PDOs and PDXOs of SGC

All established PDXs or organoids were then comprehensively genetically characterized on the basis of their transcription profiles determined using RNA-seq analysis, while the original tumors were not used due to lack of tissue. To account for the possibility of murine stromal cells contamination in PDX or PDXOs, we performed bioinformatics analysis to distinguish between human and mouse-derived reads before estimating gene expression levels (Supplementary Fig. S4), and only human-derived reads were used for analyzing the transcription profiles.

When heatmaps were obtained based on the estimated gene expression levels, each model was hierarchically clustered according to the patient origin and histological subtype (Fig. 4A). Furthermore, these results were

combined with gene expression levels of 180 cases of SGC, including multiple histological types obtained from public databases, which confirmed that our PDXs or organoids were clearly classified into each SGC histology (Fig. 4B). Correlation coefficients were then calculated between models having the same origin to quantify the similarity of these expression profiles. As shown in Fig. 4C, the gene expression levels across models having the same origin were highly correlated with mean Pearson correlation of 0.834, PDXs vs. PDOs; mean Pearson correlation of 0.871, PDXs vs. PDXOs; and mean Pearson correlation of 0.851, PDOs vs. PDXOs.

Next, we explored the presence of fusion genes using RNA-seq data. In addition to the previously reported *MYBL1-NFIB* gene in YCU-ACC-4, the frequently reported fusion gene *CRCT1-MAML2* was detected *in silico* in all PDXs, PDOs, and PDXOs of YCU-MEC-24. Moreover, its presence was reconfirmed using RT-PCR and Sanger sequencing (Supplementary Fig. S3A, B).

Genomic variation in PDXs, PDOs, and PDXOs of SGC

Since the present study did not have access to sufficient primary tumor tissues or patient blood samples for genome sequencing, we performed a limited analysis of genomic variation in the established models using RNA-seq data. The SNP and indel output according to GATK[27]. Best Practice (<https://software.broadinstitute.org/gatk/best-practices/>) were filtered by the COSMIC database[29] (<https://cancer.sanger.ac.uk/cosmic>). All extracted mutations are listed in Supplementary Table S2. Among these results, the representative genomic mutations frequently found in SGCs are also shown in Fig. 5. *TP53* mutation, frequently observed in SGC[11], was detected in all samples other than those derived from YCU-SDC-14. In contrast, *PIK3CA* mutation, which has been reported in SDC and ACC[11], was not detected in our series.

Discussion

This study is the first to report the generation of *in vitro* and *in vivo* models of multiple SGC histological subtypes using our previously established approach for organoid culture and PDX[17]. We confirmed histological as well as genetic reproducibility of our all PDXs, PDOs, and PDXOs of SGC established in this study. Thus, we showed that our established approach can be adapted for the generation of organoids and PDXs of SGC with multiple histological subtypes, whose problem of a lack of pre-clinical model systems due to its scarcity and slow-growing characteristics.

To date, there are several previous reports on the establishment of cell lines for SGC[36–41]. In terms of SDC cell line, MDA-SDC-04 is the only SDC cell line established using a 2-dimensional culture reported until now[39], while Li et al. reported that the line requires an immortalization process and loses chromosomal aberrations by long-term passaging without any tumor-forming potential in xenografts. Thus, it is difficult to establish SDC cell lines using traditional 2-dimensional culture that reproduces the original tumor characteristics. Our study is the first to report the establishment of PDXs and organoids generated from human SDC tumors with histological reproducibility of the original SDC tumor by orthotopic transplantation of SDC organoids, with its genetic reproducibility as SDC models confirmed using RNA-seq.

While most of the previous literatures reporting the establishment of SGC cell lines were based on only a single histological subtype of SGC each with a very limited number of lines, our method allowed various histological subtypes of SGCs for the culture with a certain percentage of model establishment. Furthermore, our results are consistent with previous observations that organoid culture can be applied to a number of malignancies and has been regarded as a novel culture approach that preserves more of the original tumor characteristics than the

traditional 2-dimension culture technique. However, we need to pay attention that our establishment rate of organoids or PDXs was lower than those in other malignancies such as breast cancers or lung cancers. In terms of establishment rate of SGC PDX, our result was lower compared to the previous literature by Keysar et al., presenting multiple SGC PDX[42]. This might be attributed to the different histological subtypes of SGCs included in the studies. Because we only presented the mutational status of the successfully grown cultures, we could not exclude the possibility that a specific set of mutation(s) might predispose SGC to be successfully grown as PDX and/or organoid, although we have no information on which genetic changes are associated with optimized growth either as PDX or organoid.

In the present study, we also revealed that PDX tumor could derive organoids (PDXOs) that were homologous to PDOs for SDC and MEC, as we previously presented the usability of PDXOs of ACC in our study[17]. Particularly, our PDXOs of SDC showed similar aspects of gross cyst formation and histological properties of the orthotopic transplants with similarities in gene expression. These results are also consistent with previously reported methods for PDXOs of pediatric liver cancer[43] and non-small lung cancer[44].

Our SGC organoids proliferated very slowly as do their primary tumors in some tissue types; therefore, the number of cells obtained from the culture process is limited. As PDO of YCU-MEC-24 was terminated growth during passage, the number of cells obtained from PDOs alone might be insufficient to use continuously for a variety of studies from both practical and cost perspectives. In such a case, the use of PDXO organoids is thought to be an alternative method that can overcome this issue concerning the culture of slow-growing cancers, since we confirmed that PDX was capable of multiple passages, up to a maximum of approximately eight times, while securing tumor volume as well as maintaining the model without loss.

In contrast, PDX always potentially contains mouse mesenchymal cells[45]; hence, PDXOs cultures always carry the risk of mouse cell contamination. In fact, the PDXO of YCU-SDC-20 contained a relatively large number of mouse-derived reads according to the bioinformatics analysis, and the PCR for mouse-derived mitochondrial DNA sequences was positive (Supplementary Fig. S5), suggesting that the PDXO of YCU-SDC-20 possibly contained some mouse cells. While we did not observe any significant differences in tumorigenic, histological, and genetic profiles by orthotopic transplantation between our models in the present study, these results may be affected by the proportion of mouse cells. Therefore, it is necessary to always consider the risk of contamination when conducting research using PDX-related approach.

Another limitation of the present study is that our model did not fully reflect the highly differentiated and heterogeneous nature of SGC. First, we observed small differences in protein expression patterns in IHC of PDX and orthotopically transplanted organoids. Although the primary tumor of YCU-SDC-14 was partially positive for AR, all our PDXs, PDOs, and PDXOs of YCU-SDC-14 were AR negative in this study. Meanwhile, in the case of YCU-SDC-20 with AR positive primary tumor, we observed that the transcription profiles of YCU-SDC-20 and YCU-SDC-20 PDX/YCU-SDC-20X obtained using RNA-seq analysis did not correlate well, while those of YCU-SDC-20 PDX and YCU-SDC-20X correlated very well. However, PDXs and PDOs of YCU-SDC-20 were AR negative, whereas PDX-derived tumor were somehow AR positive. These phenomena might be due to the tumor heterogeneity[46] and/or clonal selection. There was the possibility that cancer cells may evolve and selectively change their properties from those observed in the original tumor through model establishment and its passaging[47]. On the other hand, the major population expressing AR might be de-differentiated through passage in this study. Although our SDC models were not supplemented with testosterone, it was possible that the testosterone supplementation could have maintained AR expression, as shown in prostate cancer PDX models[48]. When comparing the heterogeneity of

SGCs of primary tumor and of our pre-clinical models, a major limitation of the current study is that we did not directly compare the reproducibility of gene expressions using RNA-seq or gene mutations using genome sequencing because we did not collect a sufficient amount of the primary patient tumor or other patient samples such as blood; therefore, the retention of gene expression or mutations through model establishment and its passaging was not explored in detail.

Despite these limitations, our results present the significance of SGC related organoids in a variety of histological types may be a milestone in the future development of novel therapy for SGCs. In fact, we also demonstrated that our SGC models were amenable for pharmacologic examinations *in vitro* as well as *in vivo* (data not shown). While the lack of *in vitro* and *in vivo* SGC models that recapitulate the diversity of human SGC has hampered the progress in understanding disease pathogenesis and therapy response until recently, our approach could be a powerful resource for pre-clinical SGC pharmacogenomic studies for overcoming these situations. In the future, our approach would be further expanded to more malignancies and histological subtypes with higher establishment rates by using new culture techniques such as conditional reprogramming[49].

In conclusion, we newly generated PDXs and PDOs as *in vitro* and *in vivo* models of SDC, MEC, and MYEC, in addition to ACC. Additionally, we show that PDX tumors could be used to derive organoids in SDC and MEC. We confirmed that our established PDXs, PDOs and PDXOs retain their original histological and genetical features of corresponding histological subtypes through passaging. The framework of our developed organoids and PDX-related SGC models shows potential application in preclinical studies for the development of novel treatment modalities for patients diagnosed with rare cancers, including SGC, and may be a useful tool for elucidating the molecular biology of these diseases.

Abbreviations

ACC, adenoid cystic carcinoma; DMEM, Dulbecco's Modified Eagle Medium; DNA, deoxyribonucleic acid; GFR, growth-factor-reduced; IHC, Immunohistochemistry; NSG, NOD Cg-*Prkdc*^{scid}*Il2rg*^{tm1Wjl}; MEC, mucoepidermoid carcinoma; MYEC, myoepithelial carcinoma; PDX, patient-derived tumor xenograft; RNA, ribonucleic acid; PCA, principal component analysis; PDO, patient-derived organoid; PDXO, PDX-derived organoid; RT-PCR, reverse transcription polymerase chain reaction; SGC, salivary gland carcinoma; STR, short tandem repeat.

Declarations

Authors' Contributions

Conception and design: D.S, H.T., N.O.

Development of methodology: Y.A., K.T., J.A., R.O., Y.U.

Acquisition of data: Y.A., K.T., J.A., Y.N., H.H., T.H., H.T., G.N.

Analysis and interpretation of data: Y.A, K.T., J.A., D.S, S.Y., M.S., Y.K., J.R., Y.I.

Writing, review and/or revision of the manuscript: Y.A, D.S., N.O.

Administrative, technical, or material support: Y.A., K.T., J.A, Y.N., H.H., T.H., H.T., G.N.

Study supervision: D.S., S.F., Y.S., H.T., N.O.

Funding

This work was supported by 19K09895 (PI: D.S.), 19K09873 (PI: H.T.), 21K09636 (PI: G.N.) and 21K09612 (PI: N.O.) from Japan Society for the Promotion of Science, Yokohama City University Hospital advanced medical treatment supporting system (approval No. 2019-112), the grant for 2019–2020 Strategic Research Promotion (No. SK2803) of Yokohama City University, and fund (11800122) for Creation of Innovation Centers for Advanced Interdisciplinary Research Areas Program in the Project for Developing Innovation Systems from the Ministry of Education, Culture, Sports, Science and Technology (MEXT) of Japan (H.T.).

Data availability

The RNA sequencing data that support the findings of this study have been deposited in the DNA Data Bank of Japan Sequence Read Archive (DRA) under the accession number DRA011243. All data supporting the findings of the study are available within the Article, Supplementary Information or available from the corresponding author upon request.

Ethical approval and consent to participate

The study was approved by the ethical committees of the Institutional Review Boards of the Yokohama City University (approval IDs: A171130010) and was conducted in accordance with the Helsinki Declaration; written informed consent was obtained from all patient prior to specimen collection. All animal experiments were conducted in accordance with procedures approved by the Institutional Animal Care Use Committee at Yokohama City University, School of Medicine (Yokohama, Japan).

Consent for publication

Not applicable.

Competing interests

The authors have no conflict of interest.

References

1. A.L. Carvalho, I.N. Nishimoto, J.A. Califano, L.P. Kowalski, *Int. J. Cancer* **114**, 806–816 (2005). doi:10.1002/ijc.20740
2. *2, Who Classification of Head and Neck Tumours*, 4th edn. (IARC Publications, Lyon, 2017)
3. S. Zhu, C. Schuerch, J. Hunt, *Arch. Pathol. Lab. Med.* **139**, 55–66 (2015). doi:10.5858/arpa.2014-0167-RA
4. C.C. Griffith, A.C. Schmitt, J.L. Little, K.R. Magliocca, *Arch. Pathol. Lab. Med.* **141**, 381–395 (2017). doi:10.5858/arpa.2016-0259-SA
5. E. Boon, M. Bel, W. van Boxtel, W.T.A. van der Graaf, R.J.J. van Es, S.E.J. Eerenstein, R.J. Baatenburg de Jong, M.W.M. van den Brekel, L.A. van der Velden, M.J.H. Witjes, A. Hoeben, S.M. Willems, E. Bloemena, L.A. Smit,

- S.F. Oosting, P. Group, M.A. Jonker, U.E. Flucke, C.M.L. van Herpen, *Int. J. Cancer* **143**, 758–766 (2018). doi:10.1002/ijc.31353
6. M.R. Gilbert, A. Sharma, N.C. Schmitt, J.T. Johnson, R.L. Ferris, U. Duvvuri, S. Kim, *JAMA Otolaryngol. Head Neck Surg.* **142**, 489–495 (2016). doi:10.1001/jamaoto.2015.3930
7. R.K. Sur, B. Donde, V. Levin, J. Pacella, J. Kotzen, K. Cooper, M. Hale, *Laryngoscope* **107**, 1276–1280 (1997). doi:10.1097/00005537-199709000-00022
8. S. van Weert, E. Bloemena, I. van der Waal, R. de Bree, D.H. Rietveld, J.D. Kuik, C.R. Leemans, *Oral Oncol.* **49**, 824–829 (2013). doi:10.1016/j.oraloncology.2013.05.004
9. S. Ali, M. Sarhan, F.L. Palmer, M. Whitcher, J.P. Shah, S.G. Patel, I. Ganly, *Ann. Surg. Oncol.* **20**, 2396–2404 (2013). doi:10.1245/s10434-013-2872-2
10. M. Guzzo, S. Andreola, G. Sirizzotti, G. Cantu, *Ann. Surg. Oncol.* **9**, 688–695 (2002). doi:10.1007/BF02574486
11. G. Stenman, F. Persson, M.K. Andersson, *Oral Oncol.* **50**, 683–690 (2014). doi:10.1016/j.oraloncology.2014.04.008
12. A. Nordkvist, H. Gustafsson, M. Juberg-Ode, G. Stenman, *Cancer Genet. Cytogenet.* **74**, 77–83 (1994). doi:10.1016/0165-4608(94)90001-9
13. M. Persson, Y. Andren, J. Mark, H.M. Horlings, F. Persson, G. Stenman, *Proc. Natl. Acad. Sci. U S A* **106**, 18740–18744 (2009). doi:10.1073/pnas.0909114106
14. N. Sachs, H. Clevers, *Curr. Opin. Genet. Dev.* **24**, 68–73 (2014). doi:10.1016/j.gde.2013.11.012
15. C. Pauli, B.D. Hopkins, D. Prandi, R. Shaw, T. Fedrizzi, A. Sboner, V. Sailer, M. Augello, L. Puca, R. Rosati, T.J. McNary, Y. Churakova, C. Cheung, J. Triscott, D. Pisapia, R. Rao, J.M. Mosquera, B. Robinson, B.M. Faltas, B.E. Emerling, V.K. Gadi, B. Bernard, O. Elemento, H. Beltran, F. Demichelis, C.J. Kemp, C. Grandori, L.C. Cantley, M.A. Rubin, *Cancer Discov* **7**, 462–477 (2017). doi:10.1158/2159-8290.CD-16-1154
16. J. Kondo, M. Inoue, *Cells* **8**, (2019) doi:10.3390/cells8050470
17. K. Takada, Y. Aizawa, D. Sano, R. Okuda, K. Sekine, Y. Ueno, S. Yamanaka, J. Aoyama, K. Sato, T. Kuwahara, T. Hatano, H. Takahashi, Y. Arai, G. Nishimura, H. Taniguchi, N. Oridate, *Int. J. Cancer* **148**, 193–202 (2021). doi:10.1002/ijc.33315
18. S.F. Boj, C.I. Hwang, L.A. Baker, I.I. Chio, D.D. Engle, V. Corbo, M. Jager, M. Ponz-Sarvise, H. Tiriach, M.S. Spector, A. Gracanin, T. Oni, K.H. Yu, R. van Boxtel, M. Huch, K.D. Rivera, J.P. Wilson, M.E. Feigin, D. Ohlund, A. Handly-Santana, C.M. Ardito-Abraham, M. Ludwig, E. Elyada, B. Alagesan, G. Biffi, G.N. Yordanov, B. Delcuze, B. Creighton, K. Wright, Y. Park, F.H. Morsink, I.Q. Molenaar, I.H. Borel Rinkes, E. Cuppen, Y. Hao, Y. Jin, I.J. Nijman, C. Iacobuzio-Donahue, S.D. Leach, D.J. Pappin, M. Hammell, D.S. Klimstra, O. Basturk, R.H. Hruban, G.J. Offerhaus, R.G. Vries, H. Clevers and D.A. Tuveson, *Cell* **160**, 324–338 (2015) doi: 10.1016/j.cell.2014.12.021
19. S. Pringle, M. Maimets, M. van der Zwaag, M.A. Stokman, D. van Gosliga, E. Zwart, M.J. Witjes, G. de Haan, R. van Os, R.P. Coppes, *Stem Cells* **34**, 640–652 (2016). doi:10.1002/stem.2278
20. K. Ono, M. Satoh, T. Yoshida, Y. Ozawa, A. Kohara, M. Takeuchi, H. Mizusawa, H. Sawada, *In Vitro Cell. Dev. Biol. Anim.* **43**, 168–175 (2007). doi:10.1007/s11626-007-9033-5
21. S. Chen, Y. Zhou, Y. Chen, J. Gu, *Bioinformatics* **34**, i884–i890 (2018) doi: 10.1093/bioinformatics/bty560
22. T. Conway, J. Wazny, A. Bromage, M. Tymms, D. Sooraj, E.D. Williams, B. Beresford-Smith, *Bioinformatics* **28**, i172–i178 (2012). doi:10.1093/bioinformatics/bts236

23. A. Dobin, C.A. Davis, F. Schlesinger, J. Drenkow, C. Zaleski, S. Jha, P. Batut, M. Chaisson, T.R. Gingeras, *Bioinformatics* **29**, 15–21 (2013). doi:10.1093/bioinformatics/bts635
24. Y. Liao, G.K. Smyth, W. Shi, *Bioinformatics* **30**, 923–930 (2014). doi:10.1093/bioinformatics/btt656
25. M.D. Robinson, D.J. McCarthy, G.K. Smyth, *Bioinformatics* **26**, 139–140 (2010). doi:10.1093/bioinformatics/btp616
26. J.T. Leek, W.E. Johnson, H.S. Parker, A.E. Jaffe, J.D. Storey, *Bioinformatics* **28**, 882–883 (2012). doi:10.1093/bioinformatics/bts034
27. A. McKenna, M. Hanna, E. Banks, A. Sivachenko, K. Cibulskis, A. Kernytzky, K. Garimella, D. Altshuler, S. Gabriel, M. Daly, M.A. DePristo, *Genome Res.* **20**, 1297–1303 (2010). doi:10.1101/gr.107524.110
28. P. Cingolani, A. Platts, L. Wang le, M. Coon, T. Nguyen, L. Wang, S.J. Land, X. Lu, D.M. Ruden, *Fly. (Austin)* **6**, 80–92 (2012). doi:10.4161/fly.19695
29. S.A. Forbes, D. Beare, P. Gunasekaran, K. Leung, N. Bindal, H. Boutselakis, M. Ding, S. Bamford, C. Cole, S. Ward, C.Y. Kok, M. Jia, T. De, J.W. Teague, M.R. Stratton, U. McDermott, P.J. Campbell, *Nucleic Acids Res* **43**, D805–D811 (2015). doi:10.1093/nar/gku1075
30. K. Wang, M. Li, H. Hakonarson, *Nucleic Acids Res* **38**, e164 (2010). doi:10.1093/nar/gkq603
31. Z.L. Skidmore, A.H. Wagner, R. Lesurf, K.M. Campbell, J. Kunisaki, O.L. Griffith, M. Griffith, *Bioinformatics* **32**, 3012–3014 (2016). doi:10.1093/bioinformatics/btw325
32. D. Nicorici, M. Satalan, H. Edgren, S. Kangaspeska, A. Murumagi, O. Kallioniemi, S. Virtanen, O. Kilkku, *bioRxiv*, (2014) doi: <https://doi.org/10.1101/011650>
33. H. Pimentel, N.L. Bray, S. Puente, P. Melsted, L. Pachter, *Nat. Methods* **14**, 687–690 (2017). doi:10.1038/nmeth.4324
34. P. Melsted, S. Hateley, I.C. Joseph, H. Pimentel, N. Bray, L. Pachter, *bioRxiv*, (2017) doi: <https://doi.org/10.1101/166322>
35. Y.E. Jang, I. Jang, S. Kim, S. Cho, D. Kim, K. Kim, J. Kim, J. Hwang, S. Kim, J. Kim, J. Kang, B. Lee, S. Lee, *Nucleic Acids Res* **48**, D817–D824 (2020). doi:10.1093/nar/gkz1013
36. Y. Jiang, R. Gao, C. Cao, L. Forbes, J. Li, S. Freeberg, K.M. Fredenburg, J.M. Justice, N.L. Silver, L. Wu, S. Varma, R. West, J.D. Licht, M. Zajac-Kaye, A. Kentsis, F.J. Kaye, *Oral Oncol.* **98**, 147–155 (2019). doi:10.1016/j.oraloncology.2019.09.005
37. N. Tanaka, K. Urabe, S. Hashitani, K. Sakurai, M. Urade, *Oncol. Rep.* **17**, 335–340 (2007)
38. L. Queimado, C. Lopes, F. Du, C. Martins, I. Fonseca, A.M. Bowcock, J. Soares, M. Lovett, *Int. J. Cancer* **81**, 793–798 (1999). doi:10.1002/(sici)1097-0215(19990531)81:5<793::aid-ijc21>3.0.co;2-4
39. J. Li, Y. Mitani, P.H. Rao, L. Perlaky, B. Liu, R.S. Weber, A.K. El-Naggar, *Oral Oncol.* **69**, 108–114 (2017). doi:10.1016/j.oraloncology.2017.04.007
40. A.M. Alamri, X. Liu, J.K. Blacato, B.R. Haddad, W. Wang, X. Zhong, S. Choudhary, E. Krawczyk, B.V. Kallakury, B.J. Davidson, P.A. Furth, *Dis. Model. Mech.* **11**, (2018) doi:10.1242/dmm.031716
41. K.A. Warner, A. Adams, L. Bernardi, C. Nor, K.A. Finkel, Z. Zhang, S.A. McLean, J. Helman, G.T. Wolf, V. Divi, L. Queimado, F.J. Kaye, R.M. Castilho, J.E. Nor, *Oral Oncol.* **49**, 1059–1066 (2013). doi:10.1016/j.oraloncology.2013.08.004
42. S.B. Keysar, J.R. Eagles, B. Miller, B.C. Jackson, F.N. Chowdhury, J. Reisinger, T.S. Chimed, P.N. Le, J.J. Morton, H.L. Somerset, M. Varella-Garcia, A.C. Tan, J.I. Song, D.W. Bowles, M.E. Reyland, A. Jimeno, *Clin. Cancer Res.*

- 24**, 2935–2943 (2018). doi:10.1158/1078-0432.CCR-17-3871
43. B. Bissig-Choisat, C. Kettlun-Leyton, X.D. Legras, B. Zorman, M. Barzi, L.L. Chen, M.D. Amin, Y.H. Huang, R.G. Pautler, O.A. Hampton, M.M. Prakash, D. Yang, M. Borowiak, D. Muzny, H.V. Doddapaneni, J. Hu, Y. Shi, M.W. Gaber, M.J. Hicks, P.A. Thompson, Y. Lu, G.B. Mills, M. Finegold, J.A. Goss, D.W. Parsons, S.A. Vasudevan, P. Sumazin, D. Lopez-Terrada, K.D. Bissig, *J. Hepatol.* **65**, 325–333 (2016). doi:10.1016/j.jhep.2016.04.009
 44. R. Shi, N. Radulovich, C. Ng, N. Liu, H. Notsuda, M. Cabanero, S.N. Martins-Filho, V. Raghavan, Q. Li, A.S. Mer, J.C. Rosen, M. Li, Y.H. Wang, L. Tamblyn, N.A. Pham, B. Haibe-Kains, G. Liu, N. Moghal, M.S. Tsao, *Clin. Cancer Res.* **26**, 1162–1174 (2020). doi:10.1158/1078-0432.CCR-19-1376
 45. M. Hidalgo, F. Amant, A.V. Biankin, E. Budinska, A.T. Byrne, C. Caldas, R.B. Clarke, S. de Jong, J. Jonkers, G.M. Maeldandsmo, S. Roman-Roman, J. Seoane, L. Trusolino, A. Villanueva, *Cancer Discov* **4**, 998–1013 (2014). doi:10.1158/2159-8290.CD-14-0001
 46. N. McGranahan, C. Swanton, *Cell* **168**, 613–628 (2017). doi:10.1016/j.cell.2017.01.018
 47. A.T. Pearson, K.A. Finkel, K.A. Warner, F. Nor, D. Tice, M.D. Martins, T.L. Jackson, J.E. Nor, *Oncotarget* **7**, 7993–8005 (2016). doi:10.18632/oncotarget.6919
 48. G.P. Risbridger, A.K. Clark, L.H. Porter, R. Toivanen, A. Bakshi, N.L. Lister, D. Pook, C.J. Pezaro, S. Sandhu, S. Keerthikumar, R. Quezada Urban, M. Papargiris, J. Kraska, H.B. Madsen, H. Wang, M.G. Richards, B. Niranjana, S. O'Dea, L. Teng, W. Wheelahan, Z. Li, N. Choo, J.F. Ouyang, H. Thorne, L. Devereux, R.J. Hicks, S. Sengupta, L. Harewood, M. Iddawala, A.A. Azad, J. Goad, J. Grummet, J. Kourambas, E.M. Kwan, D. Moon, D.G. Murphy, J. Pedersen, D. Clouston, S. Norden, A. Ryan, L. Furic, D.L. Goode, M. Frydenberg, M.G. Lawrence, R.A. Taylor, *Nat. Commun.* **12**, 5049 (2021). doi:10.1038/s41467-021-25175-5
 49. N. Palechor-Ceron, E. Krawczyk, A. Dakic, V. Simic, H. Yuan, J. Blacato, W. Wang, F. Hubbard, Y.L. Zheng, H. Dan, S. Strome, K. Cullen, B. Davidson, J.F. Deeken, S. Choudhury, P.H. Ahn, S. Agarwal, X. Zhou, R. Schlegel, P.A. Furth, C.X. Pan, X. Liu, *Cells* **8**, (2019) doi: 10.3390/cells8111327

Figures

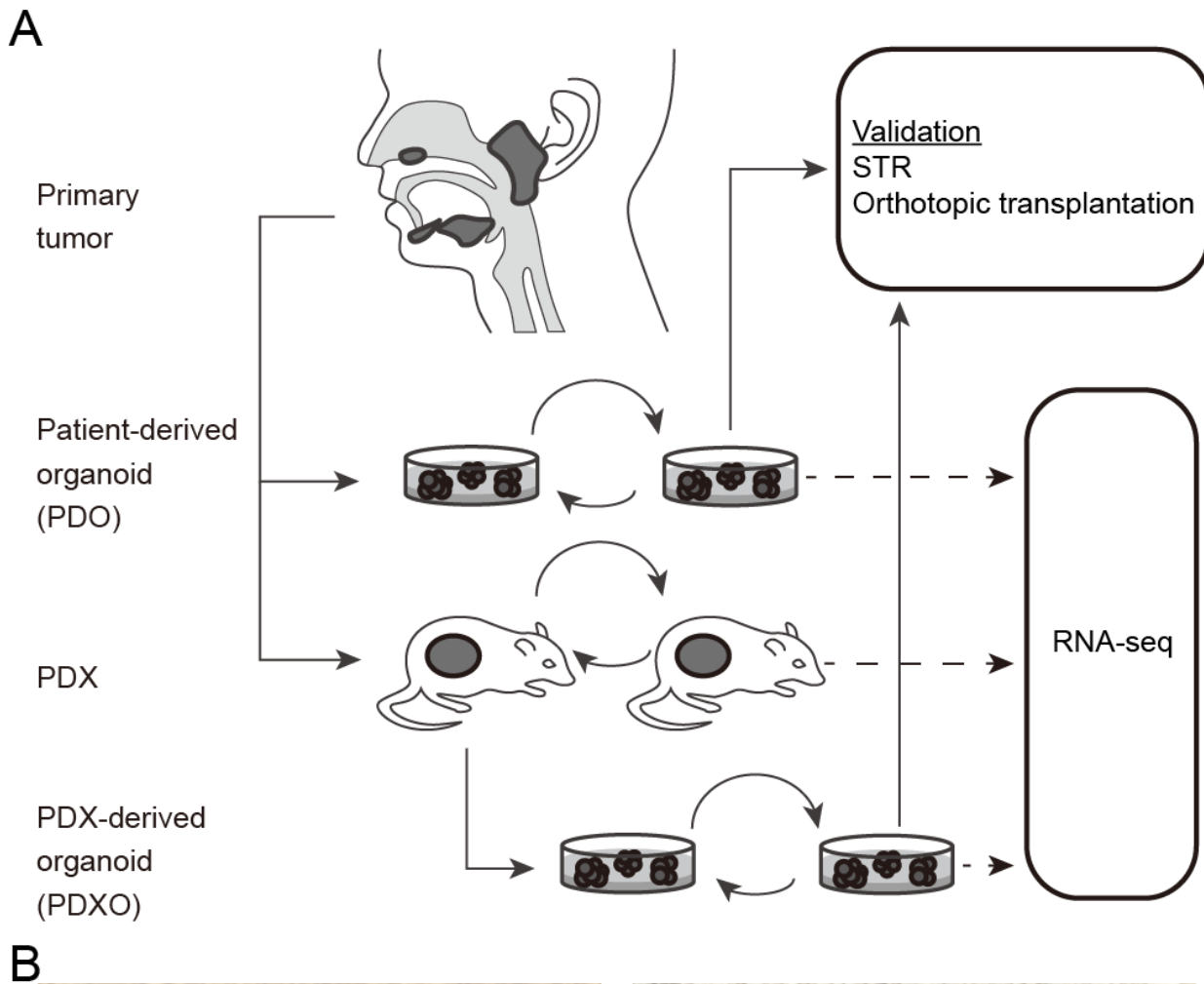


Figure 1

Establishment of salivary gland carcinoma (SGC) patient-derived xenografts (PDXs), organoids, and orthotopic transplants.

A Overview of the experiment. The patient specimens were divided into PDX and/or organoid cultures. When PDX was successfully established, we attempted to culture the PDXOs. RNA-seq was performed on all established PDXs, human tumor-derived organoids, and PDXOs, but could not be performed on the patient's primary tumor due to insufficient sample volume. **B** Representative orthotopic transplants formed in the submandibular gland of

a mouse. A PDXO from salivary duct carcinoma (YCU-SDC-20X) was transplanted into the left and right submandibular glands of the mouse and formed the tumor respectively.

Figure 2

Bright-field images and hematoxylin and eosin (H&E) staining of salivary gland carcinoma (SGC) organoids.

The left column shows the human tumor-derived organoids, and the right column shows the patient-derived xenograft (PDX)-derived organoids. The human tumor-derived organoid and PDXO derived from salivary duct carcinoma (YCU-SDC-14 series, YCU-SDC-20 series) both showed a cyst-like structure with necrosis inside. Those from mucoepidermoid carcinoma (YCU-MEC-24 series) both showed grape-like structures and glandular tuft formation. Scale bars represent 50 μ m for bright-field images and 20 μ m for H&E staining. See Fig. S1. for another salivary duct carcinoma organoid (YCU-SDC-32).

Figure 3

Histology and IHC staining

Hematoxylin and eosin (H&E) staining and IHC (CK, AR, HER2, GCDFP-15) of the patient's primary tumor, patient-derived xenograft (PDX), orthotopically transplanted PDO, and orthotopically transplanted PDXO. A case of salivary duct carcinoma (YCU-SDC-20 series) is presented as a representative. For other cases, see Fig. S2A-G. Scale bars in a large frame represent 10 microns, and those in a small frame represent 5 microns.

Figure 4

Gene expression analysis

A Heatmap. The heatmap shows the top 2000 variability genes for patient-derived xenografts (PDXs) and organoids. **B** PCA plot. The filled circles indicate the established PDX and organoid samples. Blank circles indicate gene expression data for salivary gland carcinoma (SGC) with multiple histological subtypes or normal parotid tissue downloaded from public databases. All data were corrected for batch effects based on the tissue type. **C** correlation matrix. Scatter plots of gene expression levels for each experimental model were plotted for patient samples in which the human tumor-derived organoids, PDX, and PDXOs were established (YCU-SDC-14, YCU-SDC-20, and YCU-MEC-24). The Pearson correlation coefficient and 95% confidence interval are shown in the table below.

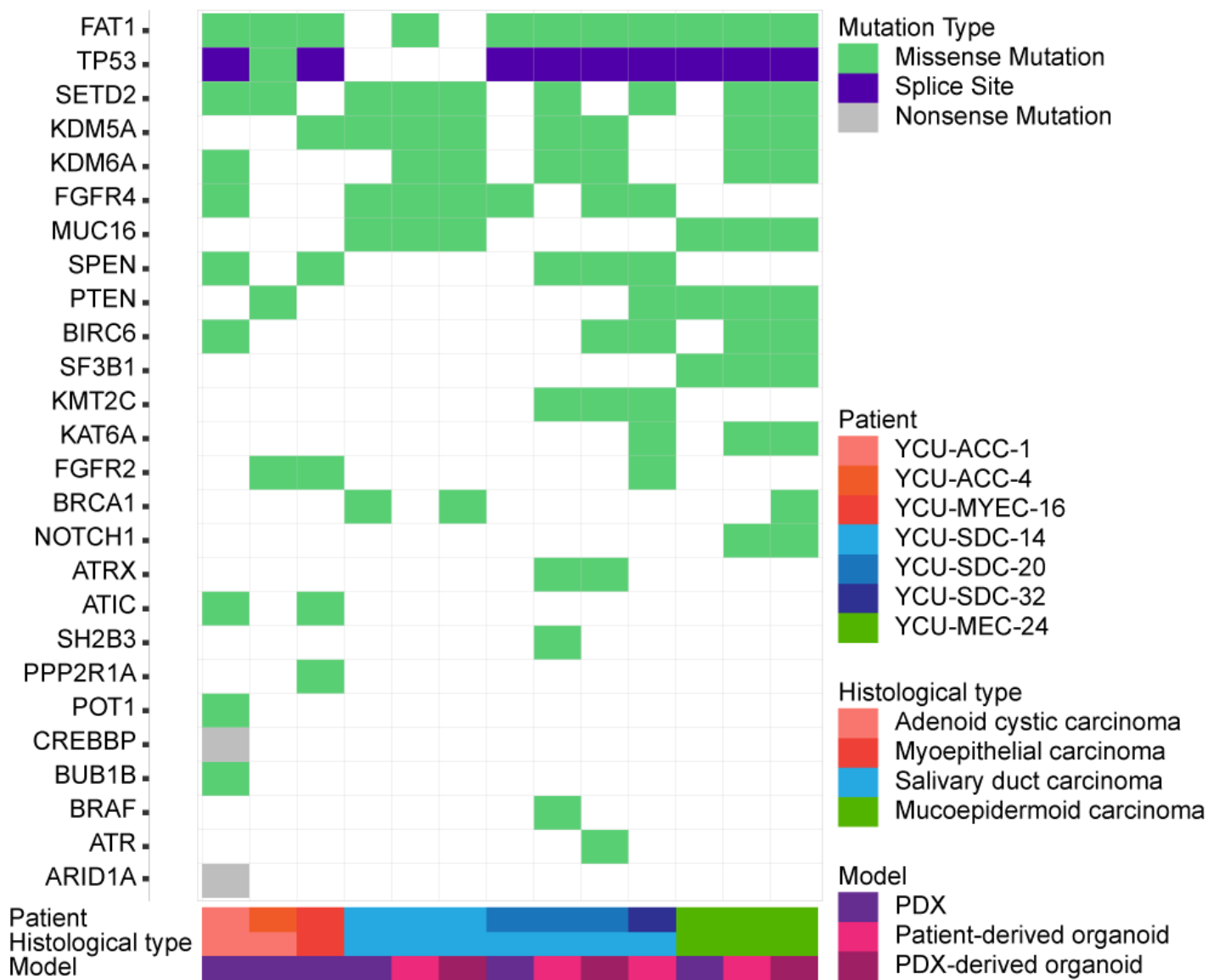


Figure 5

Gene mutation/variant analysis

Genetic variants detected in the RNA-seq data of each established model. Genetic variants were annotated, and typical possible effects on genes are shown. See Supplementary Table S2 for a list of all genetic variants.

Supplementary Files

This is a list of supplementary files associated with this preprint. Click to download.

- [Supplementarymaterials20220504.pdf](#)
- [SupplementaryTable1.xlsx](#)
- [SupplementaryTable2Valiantlist.xlsx](#)
- [SupplementaryTableS3.xlsx](#)